In Vitro Evolution of Ligands to the Membrane Protein Caveolin

Sudipta Majumdar,[†,§] Agnes Hajduczki,[‡,§] Rosemarie Vithayathil,[‡] Tivoli J. Olsen,[†] Ryan M. Spitler,[‡] Aaron S. Mendez,[‡] Travis D. Thompson,[†] and Gregory A. Weiss[*,†,‡]

[†]Department of Chemistry, and [‡]Department of Molecular Biology and Biochemistry, University of California, Irvine, California 92697, United States

Ⓢ Supporting Information

ABSTRACT: Membrane proteins comprise a third of the human genome, yet present challenging targets for reverse chemical genetics. For example, although implicated in numerous diseases including multiple myeloma, the membrane protein caveolin-1 appears to offer a poor target for the discovery of synthetic ligands due to its largely unknown structure and insolubility. To break this impasse and identify new classes of caveolae controlling lead compounds, we applied phage-based, reverse chemical genetics for the discovery of caveolin-1 ligands derived from the anti-HIV therapeutic T20. Substitution of homologous residues into the T20 sequence used a process analogous to medicinal chemistry for the affinity maturation to bind caveolin. The resultant caveolin-1 ligands bound with >1000-fold higher affinity than wild-type T20. Two types of ELISAs and isothermal titration calorimetry (ITC) measurements demonstrated high affinity binding to caveolin by the T20 variants with K_d values in the 150 nM range. Microscopy experiments with the highest affinity caveolin ligands confirmed colocalization of the ligands with endogenous caveolin in NIH 3T3 cells. The results establish the foundation for targeting caveolin and caveolae formation in living cells.
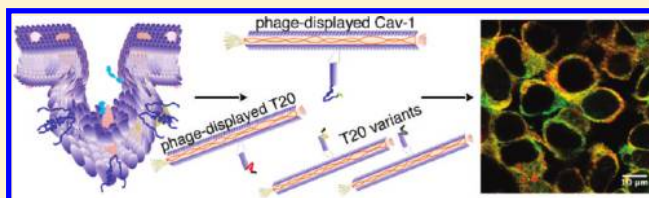
■ INTRODUCTION

Membrane proteins present challenging targets for structure determination, functional characterization, engineering, and drug development. Complicated by the inherent hydrophobicity of membrane proteins, such studies face numerous obstacles, starting with the poor expression yields of membrane proteins. In addition to ubiquity in all genomes, membrane proteins contribute key biological functions and are targets for ≥50% of currently approved therapeutics.[1] Despite recent advances in the structure determination of integral membrane proteins,[2] in vitro assays for binding and designing of ligands to membrane proteins remain difficult, idiosyncratic challenges. Thus, new approaches are required for targeting of membrane proteins, such as caveolin.

Anchored in the plasma membrane by an intramembrane domain, the monotopic subset of integral membrane proteins penetrates the leaflet of the plasma membrane, but does not span the width of the membrane. Instead, the N- and C-termini of such proteins typically remain on one side of the membrane, either the cytoplasmic or the extracellular milieu.[3] Monotopic membrane proteins offer promising, yet relatively unexplored, targets for drug development. For example, caveolin, a monotopic membrane protein, remains structurally uncharacterized, but plays critical roles in cell morphology and signaling.[4]

Flask-shaped invaginations of the plasma membrane, termed caveolae, assist with endocytosis, lipid transport, cell differentiation, and signaling.[4] The most abundant protein present in the caveolae, caveolin, regulates, in part, such physiological functions.[4b] In complex with Polymerase Transcript Release Factor (PTRF or cavin), Serum Deprivation Protein Response (SDPR), cytoskeletal proteins, and cholesterol, caveolin forms higher order oligomeric states, often exceeding 144 subunits in size.[5] The formation of such caveolin complexes shapes the caveolae. Highly conserved across vertebrate species,[6] caveolin has been implicated in muscular dystrophy, Alzheimer's disease, diabetes, vascular abnormalities, urogenital disorders, and cancer.[7] Although a tumor suppressor,[8] caveolin-1 is also overexpressed in prostate cancer, breast cancer, and Alzheimer's disease.[9] The present study focuses on caveolin-1, one of three caveolin isoforms, referred to hereafter as caveolin.

The involvement of caveolin in many diseases makes the protein an attractive therapeutic target for many diseases including multiple myeloma.[10] However, no natural or synthetic ligands specific to caveolin have been reported. The siRNA knockout of caveolin causes the disappearance of caveolae, which demonstrates the potential for control over caveolae formation by inhibiting caveolin.[11] Current approaches to modulate caveolin transcription levels and properties target sterol regulatory elements[12] and caveolar lipids (e.g., glycosphingolipids).[10] For example, the sequestration of cholesterol by filipin, nystatin, or amphotericin hinders caveolae formation.[13] However, cholesterol, a critical component of the plasma membrane and lipid rafts, participates in a variety of dynamic cellular processes (e.g., lipid transport).[14] Thus, the cholesterol sequestration strategy hinders caveolae formation, but can also disrupt other physiological functions of the cell. New classes of caveolin targeting

compounds could offer useful reagents in cell signaling studies and potential therapeutics by controlling caveolae formation.

In addition to its role in caveolae formation, caveolin binds to gp41 an envelope protein of HIV. Phage display has been used to define a caveolin binding domain (CBD1) within gp41 (residues 618−633).[15] One class of anti-HIV therapeutics targets gp41 and blocks fusion with the host plasma membrane. For example, the FDA-approved, anti-HIV therapeutic Fuzeon (termed T20) prevents viral fusions and consists of a 36-mer peptide derived from the gp41 CHR (C-terminal heptad repeat, residues 638−673).[16] The potential interaction between caveolin and T20 has not been previously examined, and, in addition to CBD1, other regions of gp41 could interact with caveolin.

Here, we report low affinity binding by T20 to caveolin and demonstrate in vitro molecular evolution of T20 variants to obtain high affinity ligands to caveolin. As previously described, the display of full-length caveolin on the phage surface requires a new type of helper phage;[17] this display enabled assay of the full-length caveolin interaction with T20. Having established caveolin−T20 binding, phage-displayed libraries of T20 variants were used for affinity maturation targeting a soluble, oligomeric caveolin with a deleted intramembrane domain. Following expression of the affinity-matured T20 variants as fusions to maltose binding protein (MBP), four independent assays (two different types of ELISA, ITC, and confocal microscopy) examined binding by oligomeric caveolin to the affinity-matured T20 variants.

■ RESULTS AND DISCUSSION

Previous analysis of the caveolin−gp41 interaction applied immunoprecipitation[15a] and SPR studies of 20-residues derived from caveolin that were fused to glutathione S-transferase.[15] The short fragment of caveolin (20 out of 172 residues) used for the in vitro SPR study reflects the difficulty expressing and assaying full-length, membrane-bound caveolin. Recent reports of successful phage display with functional, full-length membrane proteins[17] can provide a solution to this challenge. Here, for example, full-length caveolin displayed on phage could be assayed for direct binding with gp41, T20, and a 1:1 molar mixture of gp41 and T20. As shown in Figure 1, phage-displayed caveolin binds with low affinity to HIV gp41. To identify a gp41 region in addition to CBD1 critical for caveolin binding, T20 (Table 1) was also assayed. As expected for a fragment from a larger protein, T20 binds to caveolin with slightly reduced apparent binding affinity as compared to gp41. However, a 1:1 molar stoichiometry complex of gp41 and T20 bound to the phage-displayed caveolin with greatly enhanced relative binding affinity (Figure 1). Thus, a ternary complex of caveolin−gp41−T20 can form.

The observation of enhanced binding between caveolin and gp41 in the presence of T20 implicates an additional subdomain of gp41 and also suggests a model for the interaction with caveolin. With respect to the ternary model, the gp41 used in the experiment forms a well-structured α-helix, as expected[18] (Figure S1, Supporting Information). Thus, binding by the T20 peptide likely plays little role in structuring gp41, but could affect the structure of phage-displayed caveolin. The weaker binding by T20 than gp41 could indicate contributions to binding by additional regions of gp41, which do not share overlapping sequence with T20 (e.g., CBD1). Additionally, T20, unlike gp41, is unstructured in solution,[18] and the entropic penalty upon binding could decrease its relative affinity for caveolin. In summary, the sequences shared by both T20 and gp41 (Table 1), corresponding to gp41 residues 638−673, must directly interact with caveolin, as both proteins bind caveolin independently.

Although modest, the caveolin−T20 interaction suggested T20 as a peptide-based lead compound for further affinity maturation using phage-displayed libraries of T20 variants.
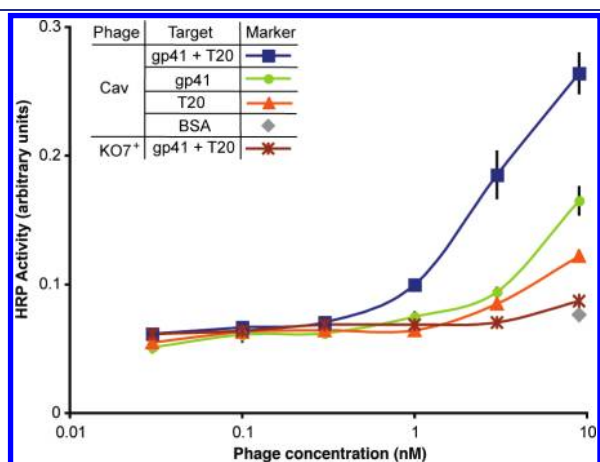

Figure 1. Direct assay of phage-displayed full-length caveolin binding to gp41 and T20. Serial dilutions of phage-displayed, full-length caveolin (Cav-1) and KO7^{+} phage not displaying a protein, as a negative control, were incubated with gp41, gp41−T20 (1:1 molar ratio), or T20 coated in microtiter plate wells. The relative levels of bound proteins were quantified by anti-M13 HRP-conjugated antibody. Caveolin binds with low affinity to T20, but T20 enhances the caveolin−gp41 interaction. In ELISAs throughout this Article, each data point represents the average of three experiments, and error bars indicate standard error.

Table 1. Sequence Homology of Caveolin Ligands Selected from Phage-Displayed Libraries[a]

T20		Y	T	S	L	I	H	S	L	I	E	E	S	Q	N	Q	Q	E	K	N	E	Q	E	L	L	E	L	D	K	W	A	S	L	W	N	W	F
gp41[b]		638										648										658										668					
Lig.	#Mut																																				
1	15	-	-	-	-	-	-	-	-	-	-	-	-	-	-	-	-	-	-	H	-	K	D	I	-	D	I	E	R	L	G	T	F	-	K	C	Y
2	9	-	-	T	-	V	K	T	-	V	D	-	-	-	-	H	-	D	R	-	-	-	-	-	-	-	-	-	-	-	-	-	-	-	-	-	-
3	9	-	-	-	M	V	K	-	-	-	D	D	T	-	Q	K	-	-	H	-	-	-	-	-	-	-	-	-	-	-	-	-	-	-	-	-	-
4	10	-	-	-	-	-	-	-	-	-	-	-	-	-	-	-	-	-	-	Q	-	K	-	-	M	-	-	E	R	-	G	-	M	L	K	C	-
5	12	-	-	-	-	-	-	-	-	-	-	-	-	-	-	-	-	-	-	H	-	K	-	I	I	D	I	E	R	-	-	-	M	L	Q	L	-
6	9	F	S	-	-	V	K	-	-	V	-	-	-	K	H	-	-	D	N	-	-	-	-	-	-	-	-	-	-	-	-	-	-	-	-	-	-
7	5	F	S	-	M	-	N	-	-	V	-	-	-	-	-	-	-	-	-	-	-	-	-	-	-	-	-	-	-	-	-	-	-	-	-	-	-

[a] Hyphens indicate conservation of the wild-type residue. Gray shading indicates the CHR region of gp41. [b] The residue numbers correspond to the positions in the gp160 of the HIV-1 HXB2 variant. Boxed residues represent the lipid-binding pocket of wild-type T20. Lig. = caveolin ligand, #Mut = number of mutations relative to the wild-type T20.
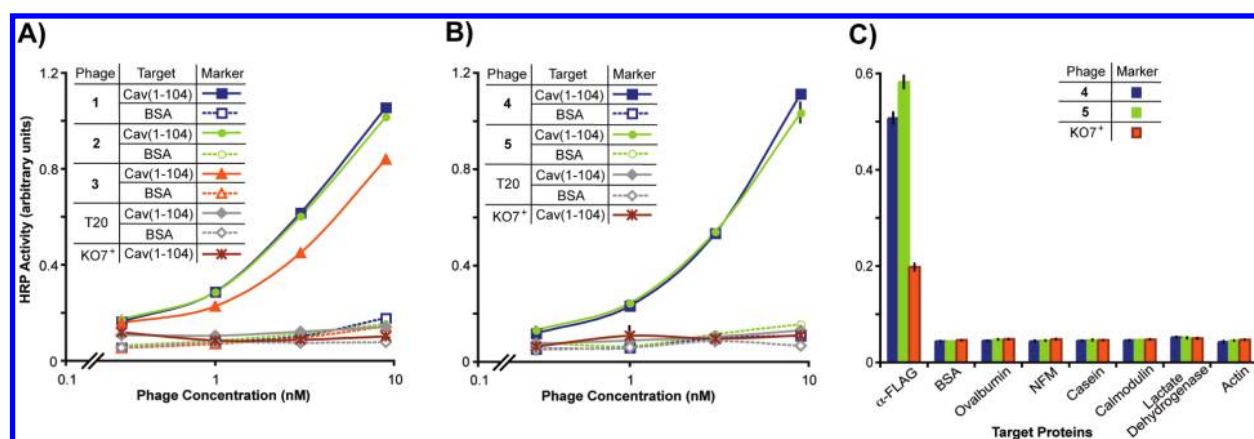
Figure 2. Phage-based ELISAs of representative T20 variants selected from the libraries. (A,B) In these experiments, the target cav(1−104) was coated on microtiter plates, and the ELISA developed as before. The selectants bound to cav(1−104) with much higher relative affinity than the wild-type T20 interaction with cav(1−104). (C) To demonstrate specificity for caveolin, ligands **4** and **5** (10 nM) displayed on KO7+ phage were assayed for binding to various negative control proteins coated on the plate and a positive control anti-FLAG antibody (α-FLAG), which can recognize a FLAG epitope fused to the N-terminus of the ligands. In this experiment, nonfat milk was used as a blocking agent. KO7+ without a displayed peptide provided a negative control for the assays.

Homologue shotgun scanning libraries, either phage- or yeast-displayed, apply combinatorial libraries with a close homologue or the wild-type residue substituted into specific positions. The approach is analogous to optimization of binding by medicinal chemistry with small changes to amino acid side chains across many positions.[19] The large size (36 residues) of T20 prevented the synthesis of a single combinatorial library. Instead, two libraries of 18 residues were designed and designated as Libraries N and C for the N- and C-terminal 18-residues of T20, respectively (Table S1, Supporting Information). The diversity of the library composed entirely of 18-residues substituted with either a close homologue or the wild-type residue ($2^{18} = 2.6 \times 10^5$) was supplemented by additional substitutions, chosen to access potentially useful mutations for affinity maturation. The two libraries had a theoretical diversity of $>10^8$ different T20 variants. As assessed by phage titers, the practical diversity of Libraries N and C were 1.2×10^9 and 3.0×10^8, respectively.

The two libraries were subjected in parallel to thermodynamic or equilibrium-based selections. Targeting a membrane protein, like caveolin, can present technical challenges to such selections. Thus, a truncated construct of caveolin (residues 1−104) with intramembrane and C-terminal domains deleted, termed cav-(1−104), was overexpressed in *E. coli* and purified to provide a robust target for the selections (Figure S2, Supporting Information). The purified protein remains functionally active, as demonstrated through binding to full-length caveolin.[20] To reduce background binding between the phage scaffold and this target, KO7+ was used as a helper phage for library synthesis. With a modified phage coat, KO7+ decreases background binding to a wide range of targets.[21] After biopanning targeted to cav(1−104), functional variants of T20 from the libraries were identified by phage-based ELISA (Table 1 and Figure 2). A total of 200 selectants were screened from the different rounds of selections, and five different T20 variants were identified that bound to cav(1−104) with higher affinity than wild-type T20 (Figure 2). Ligand 1 emerged from round 5, and ligands 2−4 were isolated from round 4. The high mutation rate (9−15 mutations per T20 variant) reflects the large number of potential solutions for binding to caveolin and the relatively conservative nature of mutations from a homologue-based library (Table 1).

Selected from Library C, ligands **4** and **5** had 10 and 12 mutations, respectively, out of 18 positions altered in the wild-type T20 sequence. Interestingly, the two ligands converged on similar, but not identical, sequences for binding to caveolin with high affinity; as described previously,[20] homologue shotgun scanning can improve binding affinity through small adjustments to a large number of residues responsible for a specific interaction. Overall, the two ligands accumulated more positively charged side chains than did wild-type T20. Such mutations could also assist with the solubility of the caveolin ligands. Although not a design consideration, this solubility enhancement was a welcome improvement to the poor solubility of T20.[22] In addition, the lipid-binding motif of T20 (residues 670−673)[23] was heavily mutated during in vitro evolution (Table 1). Here again, the directed evolution tailored ligand composition and binding specificity.

However, the selected T20 variants and wild-type, despite their largely homologous sequences, could have different display levels on the phage surface. Such differences could alter avidity effects to skew apparent binding affinity. Ligands **4** and **5**, which exhibited the strongest relative affinity in the ELISA (Figure 2B), were chosen for further study. First, an additional ELISA experiment with the two phage-displayed ligands demonstrated the specificity of their binding to caveolin, as ligands **4** and **5** failed to bind to a number of control proteins (Figure 2C). For binding assays with nonphage-displayed caveolin ligands, sequences encoding the ligands **4**, **5**, and wild-type T20 were subcloned into a modified MBP fusion vector for protein overexpression; the modifications to the vector considerably increased the yields of overexpressed T20 variants and are described in the Materials and Methods. The constructs were overexpressed as His6-tagged proteins in *E. coli*, purified to >95% homogeneity (Figure S2, Supporting Information), and first examined by ELISA for binding to various caveolin constructs. As expected, ligands **4** and **5** fused to MBP bound to phage-displayed full-length caveolin (Figure 3A and B), and also to purified cav(1−104) (Figure 3C) with much higher relative affinity than wild-type T20 fused to MBP. As a negative control, MBP failed to interact with cav(1−104). Although the two ligands exhibited roughly similar binding affinities when displayed on the phage surface
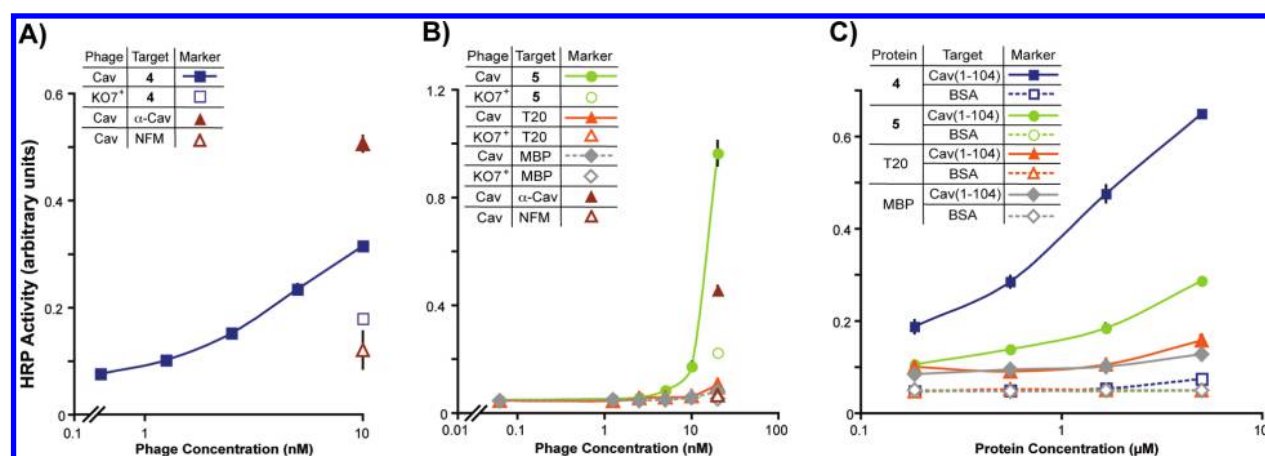
9857

dx.doi.org/10.1021/ja201792q |*J. Am. Chem. Soc.* 2011, 133, 9855–9862

Figure 3. ELISAs with overexpressed T20 variants removed from the phage surface. (A,B) Selected from phage-based affinity maturation, ligands **4** and **5** fused to MBP bound much more strongly to phage-displayed full-lenth caveolin than wild-type T20−MBP. (C) The ligands also bound to cav(1−104). MBP provided a negative control for the assay.

Table 2. ITC-Derived Thermodynamic Binding Parameters for Interactions with cav(1−104)[a]

					μM		kcal/mol		kcal/mol		kcal/(mol·K)	
protein	c-value[b]	$\chi^2 \times 10^5$	N_1[c]	N_2[c]	K_{d1}[d]	K_{d2}[d]	ΔG°_1[e]	ΔG°_2[e]	ΔH°_1[f]	ΔH°_2[f]	$T\Delta S^\circ_1$[g]	$T\Delta S^\circ_2$[g]
4	45.4	1.23	0.353	1.85	0.155	1.96	−9.11	−7.64	−20.6	44.8	−11.4	52.4
5	14.3	3.03	0.249	1.02	0.348	5.58	−8.67	−6.93	−26.1	83.9	−17.3	90.8
T20	0.051	0.371	-	-	-	-	-	-	-	-	-	-
MBP	0.088	0.084	-	-	-	-	-	-	-	-	-	-

[a] Data for MBP-fused ligands **4**, **5**, and T20 binding to cav(1−104) fit a two binding sites per caveolin binding model. MBP−T20 and the negative control MBP failed to fit to a binding model, due to their very low affinity for caveolin. [b] The c-values are for the first binding site (using K_{d1}). [c] Errors in N_1 and N_2 range from 1.0% to 4.0%. [d] Errors in K_{d1} and K_{d2} range from 5.6% to 17.2%. [e] Errors in ΔG_1 and ΔG_2 range from 1.0% to 13.8%. [f] Errors in ΔH_1 and ΔH_2 range from 1.8% to 13.8%. [g] Errors in $T\Delta S_1$ and $T\Delta S_2$ range from 1.8% to 13.8%. Hyphens indicate parameters that could not be accurately measured due to low c-values.

(Figure 2B), assays with purified ligands demonstrated the higher affinity of ligand **4**, than **5**, for both full-length and truncated caveolin. Such differences between the assays could result from higher levels of ligand **5** displayed on the phage surface, which would increase the apparent affinity of ligand **5** in the phage-based ELISA.

Next, isothermal titration calorimetry (ITC)[24] was used to determine the thermodynamic parameters for MBP-fused ligands **4** and **5** binding to cav(1−104), which were compared to the controls MBP and T20−MBP (Table 2). The negative control, MBP, bound too weakly to cav(1−104) to measure an affinity by ITC (Figure S3, Supporting Information). The measured c-value of 0.088 for the MBP−caveolin interaction reflects the maximum solubility of around 20 μM for the cav(1−104) used as a target receptor in the ITC experiments.

The T20−caveolin interaction has not been reported previously, perhaps due to the weak nature of this interaction. Similar to the negative control MBP, T20 bound cav(1−104) with a very weak affinity in the ITC assays and consequently low c-values (0.051) (Figure S3, Supporting Information). Thus, the measured thermodynamic parameters for the T20−cav(1−104) interaction have very high error. With this caveat, the ITC data for the interaction fit a two-site binding model, in which each T20 ligand binds weakly to two caveolin molecules (K_d in the sub-millimolar range). This multisite binding is consistent with the

oligomeric structure of caveolin; the cav(1−104) used in these experiments, for example, forms higher order oligomers, which can be observed and isolated by gel permeation chromatography (Figure S4, Supporting Information). T20 and variants **4** and **5** were purified as monomers and remained monomeric under the reported conditions.

As measured by ITC, ligands **4** and **5** fused to MBP bind to cav(1−104) with a two-site binding model, based upon the lowest χ^2 value for the curve fit to the isotherm (Table 2 and Figure 4). Thus, analogous to the T20−cav(1−104) interaction described above, each molecule of ligands **4** and **5** can bind to two subunits of the oligomeric cav(1−104). The stoichiometry obtained from analysis of the ITC data suggests both ligands **4** and **5** bind to the first binding site with a ratio of one ligand to approximately three caveolin receptors (N1); the second binding site has an approximately 2:1 or 1:1 ratio of ligand **4** or **5**, respectively, per caveolin (N2). This estimate is subject to error inherent to the measurement and the weaker binding affinity of the second binding site; further structural analysis is necessary to assign the stoichiometry of the interaction with greater confidence.

The association with caveolin by ligands **4** and **5** is also negatively cooperative (Figure 4). Both interactions have 10-fold stronger affinity for the first caveolin binding site than for the second site (Table 2). This negative cooperativity reflects the
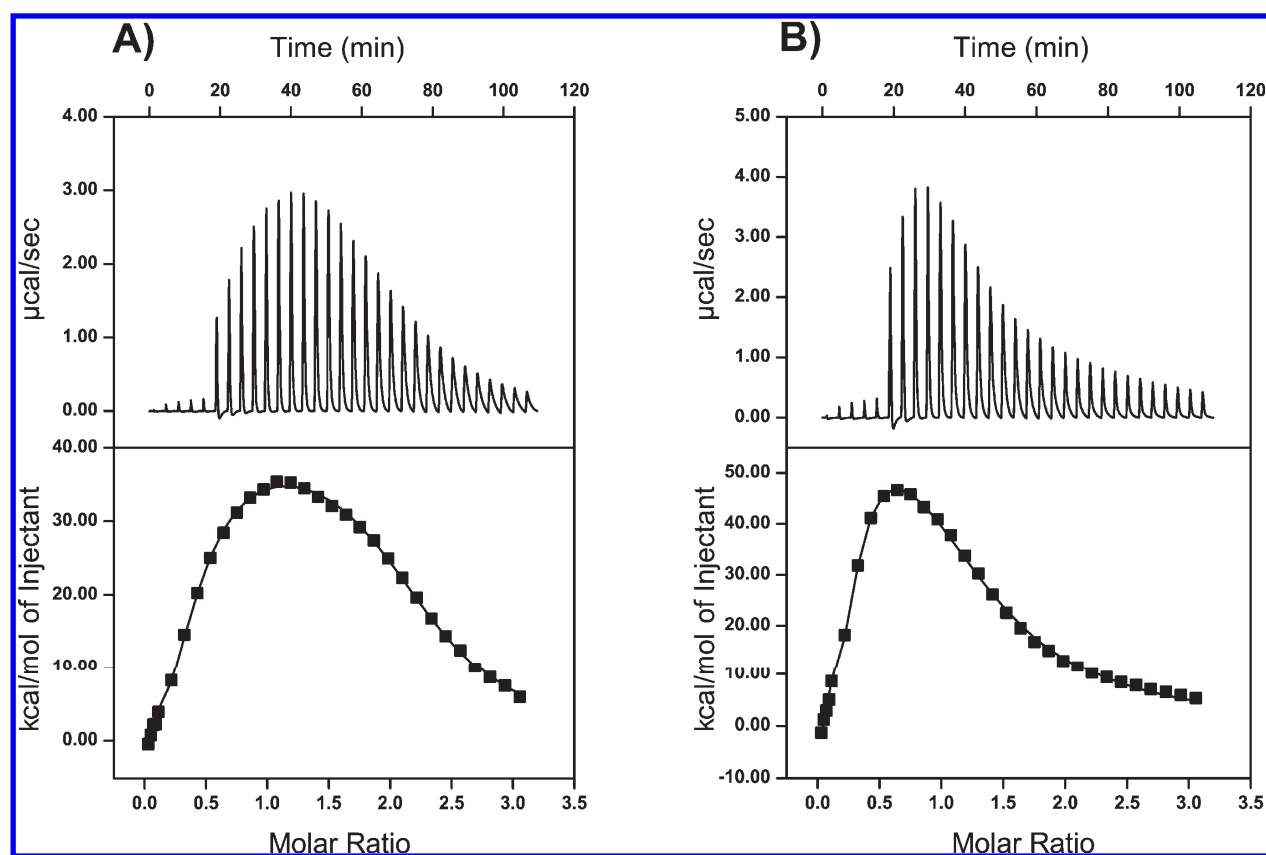
Figure 4. ITC measurements of caveolin ligands **4** and **5** binding to cav(1−104). (A) Ligand **4** or (B) **5** was injected into a solution of cav(1−104). The top graph depicts the calorimetric output for the interaction, which has been integrated in the lower graph. The molar ratio of the x-axis indicates the ratio of ligand to cav(1−104). The solid line represents the best least-squares fit for a two binding site model. Table 2 lists the thermodynamic and kinetic parameters derived from these data.

enthalpic cost for ligands **4** and **5** interacting with the second caveolin binding site, which is counter-balanced by entropic contributions. Binding to the first caveolin site by ligands **4** and **5** is exothermic; by contrast, the interaction with the second site is strongly endothermic and results in an overall endothermic binding for the two sites (Figure 4). The two-site binding to cav(1−104) by ligands **4** and **5** is entropically driven with a much greater ΔS_2 than ΔS_1 (Table 2). Such entropy-driven binding could result from disruption of the caveolin oligomers upon binding to the T20 variants or increased configurational entropy due to conformational changes in the caveolin−ligand complex.

Affinity maturation by the library design described here succeeded in producing higher affinity ligands to caveolin. From the weak estimated binding affinity for the caveolin−T20 interaction (estimated K_d of in the sub-millimolar range), both caveolin ligands **4** (K_d of 0.155 μM) and **5** protein (K_d of 0.348 μM) bound to the target with >1000-fold higher affinity. Furthermore, both ITC and ELISA data demonstrate stronger binding to caveolin by ligand **4** than by ligand **5**.

Next, we examined binding by the affinity-matured caveolin ligands in mammalian cells. Following cell fixation and permeabilization, ligands **4** or **5** fused to MBP were incubated for 6 h with NIH 3T3 fibroblasts, a cell line known to express endogenous caveolin.[5b] The presence of MBP or MBP-fused ligand was determined using a MBP-specific primary antibody followed by addition of an Alexa Fluor 488-conjugated secondary antibody. Cells incubated with MBP not fused to the caveolin ligands

served as negative controls to determine any contribution to the binding by the MBP fusion partner or the anti-MBP antibody used to label ligands **4** and **5**. To visualize endogenous caveolin, Alexa Fluor 568 conjugated to a secondary antirabbit antibody bound to a anticaveolin polyclonal antibody.

Confocal fluorescence microscopy demonstrates that both MBP-fused ligands **4** and **5** colocalize with endogenous caveolin in 3T3 cells. The yellow areas in the merged image (Figure 5A and C) highlight this colocalization. In the negative controls, cells were treated under identical conditions with MPB. The majority of the MBP protein and antibodies for visualization were washed out, indicating minimal binding to caveolin by MBP (Figure 5B and D). The colocalization of caveolin ligand **4** and caveolin was further confirmed using transient transfection of a plasmid encoding EGFP-fused to ligand **4** in NIH 3T3 cells (Figure S5, Supporting Information).

In conclusion, data from two types of ELISA, ITC, and cellular imaging demonstrate the identification of artificial, high affinity ligands to caveolin. This discovery originated with the chance observation that the anti-HIV therapeutic drug T20 binds to caveolin, albeit weakly as shown here by ITC and ELISA. Further "protein medicinal chemistry" applied a phage-based library of T20 variants with the wild-type residue, a close homologue or other substitution in every position of the initial lead. From this library, caveolin ligands with >1000-fold improvements in affinity were isolated by affinity-based selections. Further studies could examine the effects of such ligands on caveolae formation
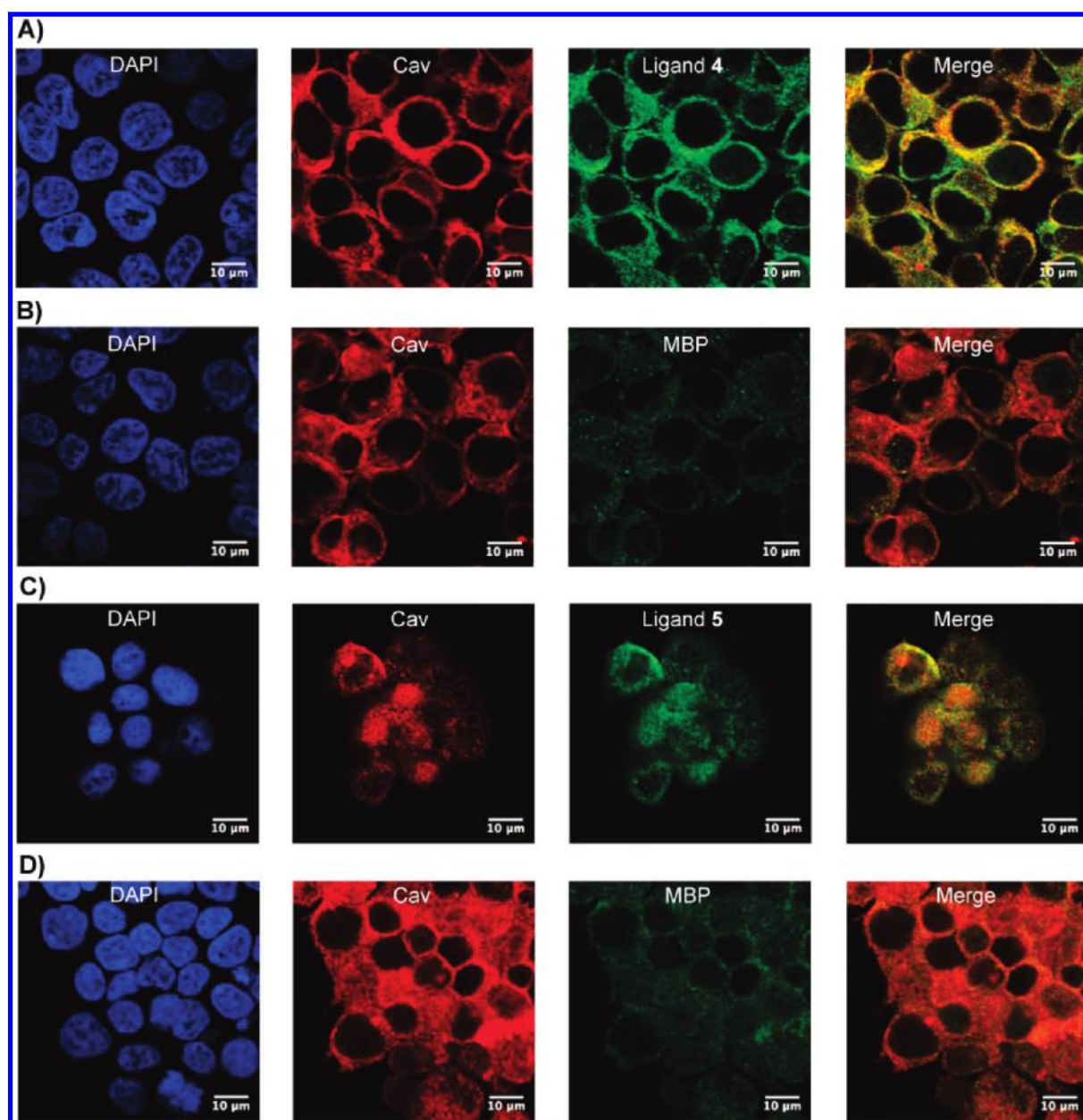
9859

dx.doi.org/10.1021/ja201792q |*J. Am. Chem. Soc.* 2011, 133, 9855–9862

Figure 5. Colocalization of caveolin-binding ligands **4** and **5** with endogenous caveolin in NIH 3T3 cells. Endogenously expressed caveolin is designated by the red signal. (A) MBP-fused ligand **4** or (B) the negative control, MBP, is labeled green, and in the merged image, the yellow regions highlight areas of colocalization. (C) Comparable experiment showing the results with MBP-fused caveolin ligand **5** with the corresponding MBP control in panel D.

and as potential therapeutics for treating multiple myeloma. As caveolae play a critical role in endocytosis, caveolin also presents a target for the development of protein transduction reagents to assist in the cellular delivery of reagents and therapeutics.

■ MATERIALS AND METHODS

Subcloning of Caveolin-1 and T20 into the Phage Display Vector. The human caveolin-1 cDNA was subcloned as described previously.[17] The T20 cDNA (NIH AIDS Research and Reference Reagent Program, Cat #1069) was amplified by PCR to incorporate *Nsi*I, *Afl*II restriction sites, and the sequence encoding a N-terminal c-Myc epitope tag (EQKLISEEDL). Analogous to the previously described procedure, the sequence encoding the c-Myc-fused T20 was subcloned into the phage display vector.[17]

Bacterial Overexpression of HIV gp41, cav(1−104), and Selected Ligands. The HIV gp41 ectodomain used for this experiment was similar, although not identical (Figure S1), to the construct described by Lu and co-workers.[25] The gp41 ectodomain with residues 546−578 and 624−655 were fused through a glycine-rich linker and expressed as previously reported.[17] A similar strategy was used to subclone residues 1−104 of caveolin-1 into the pET28c vector. Using Quikchange oligo-directed mutagenesis, the T7 epitope tag (60 base pairs) between the sequence encoding the His$_6$ sequence and either gp41 or cav(1−104) was deleted. For expression of the T20 variants from the library, phage-displaying ligands **4**, **5**, or wild-type T20 were subjected to a PCR using primers to introduce *Eco*RI and *Sal*I restriction sites. The resulting PCR products were next subcloned into a modified pET28c vector, which included the gene encoding the maltose-binding protein (MBP) between the *Nhe*I and *Eco*RI restriction sites.

9860

dx.doi.org/10.1021/ja201792q |*J. Am. Chem. Soc.* 2011, 133, 9855–9862

The vectors encoding the proteins were transformed into BL21-(DE3) *E. coli* before growth at 37 °C for 2 h. After the cells reached an OD_{600} of 0.6, addition of IPTG (0.5 mM) induced protein expression during which the cells were shaken at either 37, 25, or 30 °C, respectively, for the cav(1−104), the gp41, or the MBP constructs. Following centrifugation and sonication, protein purification typically used buffers based on a common lysis buffer (300 mM NaCl, 50 mM NaH_2PO_4, pH 8.0) with the exception of cav(1−104), which required buffer supplemented with sarcosyl (*N*-lauroylsarcosine sodium salt) (0.25% w/v). The crude lysate was incubated with the nickel-NTA resin for 2 h at 4 °C in the presence of lysis buffer with 10 mM 2-mercapto-ethanol, and the column was washed with wash buffer (lysis buffer containing 20 mM imidazole). The bound protein was eluted in lysis buffer containing 250 mM imidazole. Gel permeation chromatography further purified the proteins to >95% homogeneity.

Construction of the T20 Variant Libraries. Two libraries targeted consecutive regions of T20 from amino acid residues 638−673 (Table S1, Supporting Information). The oligonucleotides encoding Libraries N and C had theoretical diversities of 5.6×10^7 and 3.4×10^8, respectively. The actual diversities from phage titers greatly exceeded the theoretical diversity of Library N and equaled the theoretical diversity of Library C.

Construction of the T20 variant libraries used a modified version of a previously described method.[26] In brief, oligonucleotide-directed mutagenesis[27] altered the sequence encoding T20 fused to the major coat protein of M13 bacteriophage (P8). To minimize high background binding to the cav(1−104) target during selections, KO7$^+$ helper phage at a concentration of ∼1.5×10^{10} phage/mL was used to infect the bacteria culture following recovery from electroporation. The two libraries were subjected to parallel selections.

Selection of Caveolin Binding T20 Variants. Wells (24, 12, 12, 8, 8, and 4 in six rounds of selection, respectively) of microtiter plates (Nunc) were coated with 10 μg/mL cav(1−104) in 100 μL of 50 mM Na_2CO_3, pH 9.6, and incubated overnight at 4 °C on a shaker. After removal of the coating solution, 400 μL of a solution of 0.2% w/v bovine serum albumin (BSA) in phosphate-buffered saline (PBS, 140 mM NaCl, 2.7 mM KCl, 10 mM Na_2HPO_4, 2 mM KH_2PO_4, pH 8.0) was used to block the wells for 30 min on a shaker at room temperature. In successive rounds, the blocking reagent was switched to BSA, ovalbumin, or nonfat milk (NFM). The plate was then washed three times with 200 μL per well 0.05% Tween-20 in PBS. Phage were added to the wells in a buffer containing 0.2% w/v BSA, 0.05% Tween-20 in PBS. After a 1 h incubation on a shaker at room temperature, the wells were washed with 0.05% Tween-20 in PBS. The numbers of washes increased with each round from 5, 7, and 12 for the first three rounds to 18 washes for the last three rounds. The bound phage was eluted by adding 100 μL of 0.1 M HCl and shaking vigorously at room temperature for 5 min. The phage were neutralized with 33 μL of 1 M Tris-HCl, pH 8.0. Before incubation for 1 h at 37 °C, 1 mL of the eluted phage was used to infect 10 mL of log phase *E. coli* XL-1 Blue cells. Helper phage KO7$^+$ was added at ∼1.5 × 10^{10} phage/mL, and, after 1 h of incubation, the culture was transferred to 200 mL of 2YT supplemented with 50 μg/mL carbenicillin and 20 μg/mL kanamycin and shaken overnight at 37 °C.

Phage- and Protein-Based ELISAs. In the phage-based ELISA, 96-well microtiter plates (Nunc) were coated with 10−15 μg/mL of cav(1−104), gp41, or gp41−T20 (1:1 molar ratio) in 50 mM Na_2CO_3 (pH 9.6), and incubated on a shaker at 4 °C overnight. The wells were blocked with 0.2% w/v solution of BSA in PBS at room temperature on a shaker for 30 min and washed three times with wash buffer (0.05% v/v Tween-20 in PBS). Phage-displayed caveolin, T20, or T20 selectants were propagated for either one or two cycles of phage isolation, infection, and growth. The phage were then serially diluted along with a negative control (KO7$^+$) in phage dilution buffer (0.2% w/v BSA, 0.05% v/v Tween-20 in PBS). The plates were incubated with the samples at room temperature on a shaker for 1−2 h and then washed five times with wash buffer. Anti-M13/HRP conjugate (GE Healthcare) was diluted 1:5000 in the phage dilution buffer, added to the wells, and incubated for 30 min on a shaker at room temperature. The wells were washed five times with wash buffer and twice with PBS. 100 μL of a solution of 2 mg/mL *o*-phenylenediamine dihydrochloride, 0.02% w/v H_2O_2, in citric acid buffer (50 mM citric acid, 50 mM Na_2HPO_4, pH 5.0) was added to each well. After 10 min incubation, the absorbance at 450 nm was measured using a microtiter plate reader (Bio-Tek).

For the protein-based ELISA, the target protein cav(1−104) at a concentration of 10 μg/mL was used to coat wells of a microtiter plate. After blocking with 0.2% w/v BSA in PBS, the indicated concentrations of T20, ligands **4**, **5**, or equivalent molar concentrations of negative control MBP were added to the wells. Anti-MBP antibody (Sigma) and horseradish peroxidase-conjugated secondary antibody (anti-Mouse-HRP from Sigma) visualized the presence of the bound protein.

Circular Dichroism. Following overexpression and purification, the 6xHis-tagged gp41 ectodomain was dialyzed overnight in 50 mM NaH_2PO_4, pH 8.0, 150 mM NaCl. A circular dichroism spectrum of the protein (30 μM) was acquired on a Jasco spectropolarimeter (model J810) at 20 °C using a 2.0 nm bandwidth, 0.1 cm path length, 2.0 s response time, and a 50 nm/min scanning speed. The spectrum was corrected by subtraction of the equivalent measurements for the buffer. Thermal denaturation of gp41 (25 μM) was monitored by the change in ellipticity at 222 nm as a function of temperature every 0.2 °C with a 2 s response time. The T_m was estimated from the temperature resulting in 50% folded protein.

Isothermal Titration Calorimetry. The ITC experiments were performed using a VP-ITC instrument from Microcal (Northampton, MA). Six injections of 3 μL followed by 26 injections of 10 μL each of the ligand solution (MBP, MBP-fused T20 wild-type or variants) were added by a computer-controlled microsyringe at intervals of 210 s into the sample solution of cav(1−104) with stirring at 307 rpm. With ligands at a concentration of 300 μM and target cav(1−104) at 20 μM concentration, titrations were conducted at pH 8.0 in PBS at 20 °C. The experimental data were fit to a theoretical titration curve using software supplied by Microcal with ΔH (binding enthalpy kcal mol^{-1}), K_d (dissociation constant), and N (number of ligands binding per caveolin), as adjustable parameters. Thermodynamic parameters were calculated from the Gibbs free energy equation, $\Delta G = \Delta H - T\Delta S = -RT \ln K_a$, where ΔG, ΔH, and ΔS are the changes in free energy, enthalpy, and entropy of binding, respectively, T is the absolute temperature, and $R = 1.98$ cal mol^{-1} K^{-1}.

Cell Culture and Transfection. Ligand **4** fused to EGFP at the N-terminus was subcloned into a modified pEF6/Myc-His vector (Invitrogen) using the restriction sites *Kpn*I and *Eco*RI. The vector included a SV40 ori and EF-1α as the promoter for expression of ligand **4** fused to EGFP inside cells. The transfection into NIH 3T3 fibroblasts (ATCC) used purified DNA (5−10 μg) and a calcium phosphate coprecipitation method (Clonetech #631312). NIH 3T3 cells were propagated in DMEM media (GIBCO #11965) supplemented with antibiotics, glutamine, nonessential amino acids, and 10% v/v fetal calf serum. Cells were grown for 36 h after transfection at 37 °C, 5% CO_2, and 95% humidity.

Immunofluorescence and Microscopy. Cells were next fixed with 4% formaldehyde (Sigma) for 20 min on ice, and then permeabi-lized with a 1:1 mixture of cold methanol and PBS on a glass slide with incubation on ice for an additional 20 min. For the experiments with exogenously added ligands, blocking with 0.2% w/v BSA and 2% w/v NFM in PBS (1 h at room temperature) was followed by incubation with 6.5 μM MBP, MBP-fused ligand **4**, or MBP-fused ligand **5** for 6 h at 4 °C before washing three times with PBS and the addition of the pimary antibodies. To detect MBP, the primary antibody (mouse anti-MBP, Sigma) was diluted 1:800 in blocking buffer, and the caveolin-specific

9861

dx.doi.org/10.1021/ja201792q |*J. Am. Chem. Soc.* 2011, 133, 9855–9862

primary antibody (rabbit anticaveolin, Sigma) was diluted 1:500 dilution in blocking buffer and incubated 24 h at 4 °C at a slow shaking speed. Excess antibody was removed by washing three times with wash buffer (PBS containing 0.1% Tween-20). To detect the primary antibody, the samples were incubated for 1 h with a mixture of Alexa Fluor 488-labeled goat antimouse (Invitrogen) and Alexa Fluor 568-labeled donkey antirabbit (Invitrogen) secondary antibodies, which were both diluted 1:500 in blocking buffer and incubated for 2 h at room temperature. The slides were next washed three times with wash buffer, and then sealed by a coverslip following application of DAPI-supplemented (4′,6-diamidino-2-phenylindole) fluorescent mounting medium. Confocal imaging was performed with an Olympus Fluoview FV1000 laser scanning microscope using a 60× oil immersion objective (1.3 numeric aperture). The EGFP-expressed ligand **4** and the Alexa Fluor 488 were excited with an argon laser at 488 nm, and emission was monitored using a 505−530 nm bandpass filter. For Alexa Fluor 568 visualization, a HeNe laser at 543 nm and a 560−615 nm bandpass filter were used.

■ ASSOCIATED CONTENT

ⓢ Supporting Information. Additional supporting documents and experiments, including information about the library design, CD analysis of the HIV gp41 construct, SDS-PAGE of the proteins used for ITC, ITC measurements of MBP and T20 binding to cav(1−104), gel permeation chromatography analysis of cav(1−104) and MBP−**4**, and confocal microscropy with EGFP-fused caveolin ligand **4**. This material is available free of charge via the Internet at http://pubs.acs.org.

■ AUTHOR INFORMATION

Corresponding Author
gweiss@uci.edu

Author Contributions
§These authors contributed equally.

■ ACKNOWLEDGMENT

■ REFERENCES

(1) Russell, R. B.; Eggleston, D. S. *Nat. Struct. Biol.* **2000**, *7*, 928–930.

(2) White, S. H. *Nature* **2009**, *459*, 344–346.

(3) Blobel, G. *Proc. Natl. Acad. Sci. U.S.A.* **1980**, *77*, 1496–1500.

(4) (a) Sargiacomo, M.; Sudol, M.; Tang, Z.; Lisanti, M. P. *J. Cell Biol.* **1993**, *122*, 789–807. (b) Parton, R. G.; Simons, K. *Nat. Rev. Mol. Cell Biol.* **2007**, *8*, 185–194.

(5) (a) Murata, M.; Peranen, J.; Schreiner, R.; Wieland, F.; Kurzchalia, T. V.; Simons, K. *Proc. Natl. Acad. Sci. U.S.A.* **1995**, *92*, 10339–10343. (b) Hill, M. M.; Bastiani, M.; Luetterforst, R.; Kirkham, M.; Kirkham, A.; Nixon, S. J.; Walser, P.; Abankwa, D.; Oorschot, V. M.; Martin, S.; Hancock, J. F.; Parton, R. G. *Cell* **2008**, *132*, 113–124. (c) Hansen, C. G.; Bright, N. A.; Howard, G.; Nichols, B. J. *Nat. Cell Biol.* **2009**, *11*, 807–814. (d) Stahlhut, M.; van Deurs, B. *Mol. Biol. Cell* **2000**, *11*, 325–337.

(6) (a) Spisni, E.; Tomasi, V.; Cestaro, A.; Tosatto, S. C. *Biochem. Biophys. Res. Commun.* **2005**, *338*, 1383–1390. (b) Tang, Z.; Okamoto, T.; Boontrakulpoontawee, P.; Katada, T.; Otsuka, A. J.; Lisanti, M. P. *J. Biol. Chem.* **1997**, *272*, 2437–2445.

(7) Cohen, A. W.; Hnasko, R.; Schubert, W.; Lisanti, M. P. *Physiol. Rev.* **2004**, *84*, 1341–1379.

(8) Engelman, J. A.; Zhang, X. L.; Lisanti, M. P. *FEBS Lett.* **1998**, *436*, 403–410.

(9) (a) Yang, G.; Truong, L. D.; Timme, T. L.; Ren, C.; Wheeler, T. M.; Park, S. H.; Nasu, Y.; Bangma, C. H.; Kattan, M. W.; Scardino, P. T.; Thompson, T. C. *Clin. Cancer Res.* **1998**, *4*, 1873–1880. (b) Gaudreault, S. B.; Dea, D.; Poirier, J. *Neurobiol. Aging* **2004**, *25*, 753–759.

(10) Podar, K.; Anderson, K. C. *Cancer Lett.* **2006**, *233*, 10–15.

(11) Miyawaki-Shimizu, K.; Predescu, D.; Shimizu, J.; Broman, M.; Predescu, S.; Malik, A. B. *Am. J. Physiol. Lung Cell Mol. Physiol.* **2006**, *290*, L405–413.

(12) Bist, A.; Fielding, P. E.; Fielding, C. J. *Proc. Natl. Acad. Sci. U.S.A.* **1997**, *94*, 10693–10698.

(13) (a) Rothberg, K. G.; Ying, Y. S.; Kamen, B. A.; Anderson, R. G. *J. Cell Biol.* **1990**, *111*, 2931–2938. (b) Rothberg, K. G.; Heuser, J. E.; Donzell, W. C.; Ying, Y. S.; Glenney, J. R.; Anderson, R. G. *Cell* **1992**, *68*, 673–682. (c) Carozzi, A. J.; Ikonen, E.; Lindsay, M. R.; Parton, R. G. *Traffic* **2000**, *1*, 326–341.

(14) Hao, M.; Mukherjee, S.; Sun, Y.; Maxfield, F. R. *J. Biol. Chem.* **2004**, *279*, 14171–14178.

(15) (a) Hovanessian, A. G.; Briand, J. P.; Said, E. A.; Svab, J.; Ferris, S.; Dali, H.; Muller, S.; Desgranges, C.; Krust, B. *Immunity* **2004**, *21*, 617–627. (b) Huang, J. H.; Lu, L.; Lu, H.; Chen, X.; Jiang, S.; Chen, Y. H. *J. Biol. Chem.* **2007**, *282*, 6143–6152.

(16) Wild, C. T.; Shugars, D. C.; Greenwell, T. K.; McDanal, C. B.; Matthews, T. J. *Proc. Natl. Acad. Sci. U.S.A.* **1994**, *91*, 9770–9774.

(17) Majumdar, S.; Hajduczki, A.; Mendez, A. S.; Weiss, G. A. *Bioorg. Med. Chem. Lett.* **2008**, *18*, 5937–5940.

(18) Liu, S.; Lu, H.; Niu, J.; Xu, Y.; Wu, S.; Jiang, S. *J. Biol. Chem.* **2005**, *280*, 11259–11273.

(19) (a) Murase, K.; Morrison, K. L.; Tam, P. Y.; Stafford, R. L.; Jurnak, F.; Weiss, G. A. *Chem. Biol.* **2003**, *10*, 161–168. (b) Cochran, J. R.; Kim, Y. S.; Lippow, S. M.; Rao, B.; Wittrup, K. D. *Protein Eng. Des. Sel.* **2006**, *19*, 245–253. (c) Levin, A. M.; Murase, K.; Jackson, P. J.; Flinspach, M. L.; Poulos, T. L.; Weiss, G. A. *ACS Chem. Biol.* **2007**, *2*, 493–500.

(20) Hajduczki, A.; Majumdar, S.; Fricke, M.; Brown, I. A. M.; Weiss, G. A., submitted for publication.

(21) Lamboy, J. A.; Tam, P. Y.; Lee, L. S.; Jackson, P. J.; Avrantinis, S. K.; Lee, H. J.; Corn, R. M.; Weiss, G. A. *ChemBioChem* **2008**, *9*, 2846–2852.

(22) Xiao, J.; Burn, A.; Tolbert, T. J. *Bioconjugate Chem.* **2008**, *19*, 1113–1118.

(23) Liu, S.; Jing, W.; Cheung, B.; Lu, H.; Sun, J.; Yan, X.; Niu, J.; Farmar, J.; Wu, S.; Jiang, S. *J. Biol. Chem.* **2007**, *282*, 9612–9620.

(24) (a) Wiseman, T.; Williston, S.; Brandts, J. F.; Lin, L. N. *Anal. Biochem.* **1989**, *179*, 131–137. (b) Freire, E.; Schon, A.; Velazquez-Campoy, A. *Methods Enzymol.* **2009**, *455*, 127–155.

(25) Shu, W.; Liu, J.; Ji, H.; Radigen, L.; Jiang, S.; Lu, M. *Biochemistry* **2000**, *39*, 1634–1642.

(26) Sidhu, S. S.; Lowman, H. B.; Cunningham, B. C.; Wells, J. A. *Methods Enzymol.* **2000**, *328*, 333–363.

(27) Kunkel, T. A. *J. Biol. Chem.* **1985**, *260*, 5787–5796.

9862

dx.doi.org/10.1021/ja201792q |*J. Am. Chem. Soc.* **2011**, *133*, 9855–9862